Scientific Research Publishing

Materials Sciences and Applications, 2025, 16(3), 121-140
https://www.scirp.org/journal/msa
ISSN Online: 2153-1188
ISSN Print: 2153-117X

Sustainable Composite Based on Recycled Poly (Ethylene Terephthalate) Embedded with Titanium Phosphate/Zinc/Silver Nanofiller: Physico-Chemical Evaluations

Enzo Erbisti Garcia[1*], Gerson Alberto Valencia Albitres[1], Daniela de França da Silva Freitas[1], Sibele Piedade Cestari[2], Luis Claudio Mendes[1]

[1]Institute of Macromolecules, Federal University of Rio de Janeiro, Rio de Janeiro, Brazil
[2]Innovation in Polymer Engineering (PIEP), University of Minho, Guimarães, Portugal
Email: *enzoerbisti@ima.ufrj.br

How to cite this paper: Garcia, E.E., Albitres, G.A.V., Freitas, D.F.S., Cestari, S.P. and Mendes, L.C. (2025) Sustainable Composite Based on Recycled Poly (Ethylene Terephthalate) Embedded with Titanium Phosphate/Zinc/Silver Nanofiller: Physico-Chemical Evaluations. *Materials Sciences and Applications*, **16**, 121-140.
https://doi.org/10.4236/msa.2025.163007

Received: January 25, 2025
Accepted: March 7, 2025
Published: March 10, 2025

Abstract

Considering the commitments outlined in the United Nations 2030 Agenda, as well as the principles of recycling and the Circular Economy, this work aimed to develop a new material with enhanced properties and added value from post-consumer poly (ethylene terephthalate) (rPET) bottles. Extruded composites based on rPET were loaded with pristine titanium phosphate (TiP) and TiP modified with zinc and silver salts. The rheological assessment showed variation at low frequencies. A reduction in the contact angle was detected with the addition of fillers. No variation in rPET crystallization was observed using optical microscopy. The fillers did not affect the lightfastness. Some stiffening of the rPET amorphous phase was noted, but the damping ability of rPET remained unchanged. The material is believed to offer multifunctional feasibility for the textile sector, potentially acting as a light stabilizer and antimicrobial agent. The work endorses the principles of sustainability and confirms the suitability of recycling as a means to reduce the impact of post-consumer plastics.

Keywords

Recycled Poly (Ethylene Terephthalate), Titanium Phosphate, Recycling, Circular Economy

1. Introduction

Since the middle of the 20th century, fossil plastics have become indispensable for contemporary society. Nowadays, there is an abundance of plastic waste due to its widespread use in daily life. Concern about environmental preservation has been on the agenda of governments, civil society, and environmental organizations. Commitments included in the United Nations' 2030 Agenda, objectives in the European Union's strategies for plastics in a circular economy, recycling and other assertive attitudes aim to promote planetary sustainability [1] [2].

Under ordinary conditions, commodity fossil plastics are strong and resistant to microorganisms and moisture, and long-lasting. Recycling is one of the most feasible methods to decrease the substantial contribution of post-consumer solid plastics to municipal solid waste [3] [4].

Among the commodity plastics, poly (ethylene terephthalate) (PET) competes with polyolefins (polyethylene and polypropylene). PET possesses remarkable properties such as high strength, low density, non-biodegradability, resistance to certain chemicals, and high processability [5].

Mechanical recycling of post-consumer PET bottles has been the most widely used method for their upcycling [6] [7]. The study of post-consumer PET is widespread in the academic sector. Singh *et al*. and Lee *et al*. investigated the effect of rPET fiber as a reinforcing agent in mortar composites [8] [9]. They reported an increase in the mortar's fracture energy between 188% - 802%. Duan *et al*. published a review on recycled plastic fiber as a reinforcement in mortar/concrete formulations and its impact on mechanical properties [10]. Recycled PET in powder, pellet and fiber forms, was incorporated into cement mortar. The mechanical characteristics of the formulations depended on the amount and form of the rPET added [11].

The flame retardancy study of composites based on rPET and bio-based alginate fibers was conducted by Weng and Zhang [12]. A flame retardancy index higher than 26 and smoke emission lesser than 27% were attained. Masonry veneers were developed by Paredes *et al*. through the combination of concrete, crushed rPET, and aggregate [13]. When compared to its commercial counterpart, an improvement of 110% in flexural strength and 94% in compression strength was reported.

Maladeniya *et al*. performed a single-stage chemical recycling of PET waste by the transesterification-thiocracking process [14]. The authors reported that PET waste, geraniol, and elemental sulfur were mixed and heated. This route promoted transesterification concomitantly to the cracking of the PET backbone, leading to the formation of a crosslinked composite. Zhang *et al*. explored a depolymerization method for PET from different sources of waste [15]. By solvolysis with a mixture of dichloromethane and ethanol, terephthalic acid and ethylene glycol, monomers were yielded.

Unsaturated polyester resin (rPET-UPR) derived from PET waste was filled with graphene nanoplatelets (GPnP). It was mentioned that a reduction in the

hysteresis loop area and a slower rate of stiffness degradation suggested the retardation of fatigue damage [16]. Nanofibrous composites based on rPET and graphene nanoplatelets were produced by Kalaoglu-Altan and co-authors [17]. It was reported that there was an improvement in thermal conductivity and heat dissipation. Nasir prepared rPET composites filled with fly ash [18]. In general, thermal behavior improved, but degradation, presence of voids, and agglomeration were observed at high filler content.

Consecutively, Lopez and Smith experimented with PET chemical glycolysis, oleoyl chloride esterification, and sulfur vulcanization [19]. The authors stated that the compressive and flexural strengths attained values required for residential building foundations, similar to those of Portland cement. Brick sand was incorporated into PET waste resulting in composites. It was registered that thermal degradation and glass transition temperature increased, while impact resistance decreased as the filler content increased. Moulai *et al.* and Adiyanto *et al.* developed an eco-brick consisting of recycled PET and epoxy resin [20] [21]. The study considered the proportion of rPET to epoxy resin and the curing time. The best compressive properties were attained for rPET: Epoxy resin ratio of 10:90, with a curing period of 6.9 days.

Nanofillers possess unique properties and have been utilized in the development of polymeric nanocomposites. Lamellar nano-phosphates have gained importance and have been widely studied due to their excellent physical and chemical properties. Their structural arrangement allows for intercalation with different substances, and their insertion into polymer matrices results in materials with outstanding properties [22]-[25].

Over the last decade, our research group has devoted interest to the synthesis and intercalation of zirconium and titanium phosphate for application in polymer composites. Mendes *et al.* studied the influence of long chain amine in the structural arrangement of zirconium phosphate [26]. According to the ZrP: amine ratio, an intercalated or exfoliated structure was achieved. Albitres *et al.* investigated the effect of titanium phosphate on the thermal, crystallographic, molecular mobility, and UV-Vis absorption characteristics of PET composites [27]. The hygroscopicity change of polyamide-6/zirconium phosphate composites was studied by Garcia and collaborators [28]. Recently, an article on the action of zirconium phosphate as a flame retardant in composites based on recycled polyethylene was published [29]. Garcia *et al.* experimented with the chemical modification of titanium phosphate using zinc and silver ions, searching for a polyfunctional filler [30]. The synthesis and characterization of lamellar zirconium phosphate with the incorporation of nano-zinc oxide was developed by Mariano and collaborators [31]. Freitas *et al.* investigated reinforced composites of polyamide-6/lamellar zirconium phosphate. Mechanical, thermal, and rheological properties were registered [32].

As a premise for environmental sustainability, this work aimed to develop a composite from rPET filled with titanium phosphate modified with zinc and silver

salts. It is supposed that a new material with improved properties and added value was attained. This research aligns with the 2030 Agenda of the UN and global organizations involved with sustainability and planet preservation. Additionally, it can be viewed as an assertive action for reducing the impact of post-consumer plastics.

2. Experimental

2.1. Materials

Post-consumer poly (ethylene terephthalate) (rPET) from beverage bottles was used. Phosphoric acid (85% wt./mL), titanium isopropoxide (97%), ethanol (99%), ethylamine (70%), pyromellitic acid (96%) and zinc acetate were purchased from Sigma-Aldrich. Silver nitrate was obtained from Isofar. Two commercial dyes (red and violet) were purchased from Guarany Ind. e Com. Ltda and used as received.

2.2. Synthesis and Chemical Modification of Nano-Titanium Phosphate (TiP)

The synthesis and chemical modification of titanium phosphate have already been described previously [30] but will be briefly mentioned as follows. Under vigorous stirring, titanium isopropoxide was added dropwise into the phosphoric acid at a 1:8 molar ratio. Sequentially, deionized water was added, and the system was heated to 120˚C and maintained at that temperature for 24 hours. Thereafter, the medium was washed until the pH reached 6 and then dried in an oven at 90˚C. TiP modification was sequentially conducted with ethylamine, pyromellitic acid, zinc acetate and silver nitrate. Intercalation was performed by using ethanol and water as solvents, according to the solubility of each precursor. In each step, the final product was labeled as TiP/EA (ethylamine), TiP/EA/AP (ethylamine/pyromellitic acid), TiP/EA/AP/Zn (ethylamine/pyromellitic acid/zinc) and TiP/EA/AP/Zn/Ag (ethylamine/pyromellitic acid/zinc/silver).

2.3. rPET Processing, Masterbatch and Composite Preparation

Colorless, transparent, and multilayer bottles were collected, washed, dried, cut into flakes and ground. A portion was preserved as a blank. The remaining flakes (10 × 5 × 0.20 mm) were extruded in a twin-screw extruder Teck Trill DCT-20, at 300 rpm, within aprocessing window from 90˚C to 250˚C, resulting in pellets. To improve the filler dispersion, a masterbatch was prepared using the initial flakes combined with fillers (pristine TiP and modified - TiPEAAPZnAg), resulting in a compound with an rPET/filler ratio of 95/5 wt.%. The processing was conducted in a Haake Rheocord 9000 mixing chambe, at 240˚C, 50 rpm, for 5 minutes. The material was cut into pellets. The composite was prepared by mixing processed rPET with masterbatch to attain a final composition with 1 wt.% of filler. The processing was using a Haake model Rheocord 9000 single-screw extruder at 30 rpm, with 4 heating zones (processing window of 210˚C - 240˚C), generating fil-

ament. For aging, polarized optical microscopy, dynamic-mechanical analysis and contact angle evaluations, film specimens (25 × 15 × 0.16 mm) were prepared using a Marconi press model MA 098/A, at 250˚C, under 6 tons of pressure, for 6 minutes.

2.4. Raman Spectroscopy

Raman spectroscopy was performed using a DXR Raman Microscope equipped with a laser at a wavelength of 532 nm and a 50x lens, in the range of 200 - 4000 cm^{-1}. The vibrational modes of the samples were evaluated.

2.5. Hydrogen Nuclear Magnetic Resonance at Time Domain (^{1}HNMRTD)

^{1}HNMRTD relaxation time distribution (T2H) was obtained using the Ostroff-Waugh (OW4) pulse sequence. The analysis was performed with a recycle time of 2 s and 30˚C. The results were expressed as distribution domain curves.

2.6. Rheology

The rheology measurements were conducted using a TA rheometer, model AR-2000, with parallel plate geometry of 25 mm diameter, at 270˚C, under an inert atmosphere and oscillatory regime. A strain sweep test was performed at a frequency of 1 Hz to determine the region of linear viscoelasticity. The storage and loss moduli, as well as the complex viscosity, were assessed.

2.7. Ultraviolet Stabilization

The film was exposed to UV lamps emitting a wavelength of 365 nm for 120 hours in a UV darkroom model SP-204. Before and after aging, the sample surface underwent FTIR analysis, using a Perkin-Elmer Frontier MIR/FIR equipment, at a spectral range of 4000 - 400 cm^{-1}, by attenuated total reflectance (ATR), using 60 scans and resolution of 4 cm^{-1}. To monitor stabilization, the carbonyl index was determined considering the carbonyl band at 1723 cm^{-1}, characteristic of the rPET ester group, and the reference band at 2962 cm^{-1}. The average of four replicates was considered.

2.8. Polarized Optical Microscopy (POM)

POM was conducted using an Olympus SZH10 microscope, coupled with an HDCE-50B camera and LinKam hot stage. The film specimen was prepared by pressing the sample between glass plates under the action of heating. Before the crystallization process, photographs were taken with and without polarized light. After that, the sample was heated to 260˚C at 10˚C/min, held for 2 minutes to erase the thermal history, cooled to 200˚C and allowed to crystallize for 3 hours. Finally, the sample was cooled to room temperature and photographs were taken again with and without polarized light.

2.9. Dynamic-Mechanical Analysis (DMA)

DMA analysis was carried out using a TA Instruments Q800 instrument in tension film mode with a rectangular specimen measuring 9 × 3.2 × 1 mm. The analysis was conducted from 25˚C to 200˚C, at a heating rate of 3˚C min^{-1} and frequency of 1 Hz. Storage modulus (E'), loss modulus (E") and tangent delta (tan δ) were determined.

2.10. Contact Angle

The contact angle was measured using OCA 15 EC equipment. Water was the test liquid with a dosing rate of 0.5 μL/s. The contact angle was recorded, and its value was calculated by a computational program. The result represents the average of three determinations.

2.11. Fourier Transform Infrared Spectroscopy (FTIR)

Before infrared analysis, 5 grams of each dye were dissolved in 50 mL of acetone and allowed to stand for 24 hours. After that, the solution was filtered, and the colored liquid was subjected to FTIR evaluation. The infrared analysis was conducted in a Perkin-Elmer Frontier model equipment, from 4000 - 500 cm^{-1}, with 60 scans and a resolution of 4 cm^{-1}. The resultant spectrum was compared with those in the equipment's spectrum collection.

2.12. Light Fastness Measurement

The rPET and composites were dyed. Approximately 1.3 g of each sample was packed into a polyamide bag. On a hot plate, a three-neck flask equipped with a reflux apparatus was filled with 300 mL of distilled water and a packed sample. The mixture was heated to 60˚C under magnetic stirring at 175 rpm. The device was maintained for 10 minutes. After that, 8 grams of dye were added. The mixture was kept for an additional 10 minutes. The temperature was gradually raised to 100˚C and the mixture was kept at this temperature for 40 minutes. The system was allowed to cool down to ambient temperature. Finally, the packed sample was removed, washed with distilled water, and dried in an oven until a constant weight was achieved. The degree of fading was evaluated according to AATCC 16-2004 using an SDL-Atlas Ci 3000 + Xenon Fade-Ometer with a wavelength of 420 nm, at 1 rpm, and relative humidity of 31.6%, using a gray scale for color assessment.

3. Results and Discussion

3.1. Raman Spectroscopy

Figure 1 shows the TiP, $Zn(Ac)_2$, $AgNO_3$ and TiPEAAPZnAg. As main vibration modes of $Zn(Ac)_2$ were found at 1457 cm^{-1} (C=O stretching in bidentate coordination), 953 cm^{-1} (C-C vibration in H_3-C-C(=O)-O^-), 693 cm^{-1} (C(=O)-O^- vibration) (410 (Zn-O vibration) [33]-[35]. For $AgNO_3$ an intense vibration was assigned at 1043 cm^{-1} (Ag-O vibration) [36]. TiP presented vibrations at 1139 cm^{-1} (P-O-H in-plane deformation), 1008 cm^{-1} (PO_4^- symmetric stretching), 423 and

324 cm^{-1} (PO_4^- torsional vibration and water molecule angular deformation, respectively) and 227 cm^{-1} (PO_4^{3-} rotation R' lattice mode) in agreement with published by Slade *et al*. and Janusz *et al*. [37] [38]. For TiPEAAPZnAg, TiP vibrational mode at 1008 cm^{-1} was shifted and split into 1030 and 969 cm^{-1} and the vibration at 324 cm^{-1} was displaced to 344 cm^{-1} (see side window). Vibrational modes at 1460, 1410 and 951 cm^{-1} attributed to the zinc acetate remained. New vibrations at 1600, 1550 and 1350 could be associated with the formation of zinc and silver carboxylate salts [30]. These Raman shifts were ascribed to the O=C-O asymmetric and symmetric vibrational modes as referred to by Diniz *et al*. and Pan *et al*. [39] [40]. **Figure 2** shows spectra of rPET, rPET/TiP and rPET/TiPEAAPZnAg. For all samples, rPET multiple vibration modes were assigned at 3100 - 2900 cm^{-1} (C-H vibration), 1726 cm^{-1} (C=O ester vibration), 1614 cm^{-1} (C=C aromatic ring vibration), 1300 - 1000 cm^{-1} (O=C-O and O-C-O vibration) and below 900 cm^{-1} vibrations associated with C-C benzene ring and C-H out-of-plane [41]-[43]. In summary, Raman analysis of the fillers was carried out to show the successful modification of TiP using zinc acetate and silver nitrate salts. The amount of filler used in the composites was 1 wt.%, which was believed to be too low to be detected by this technique.

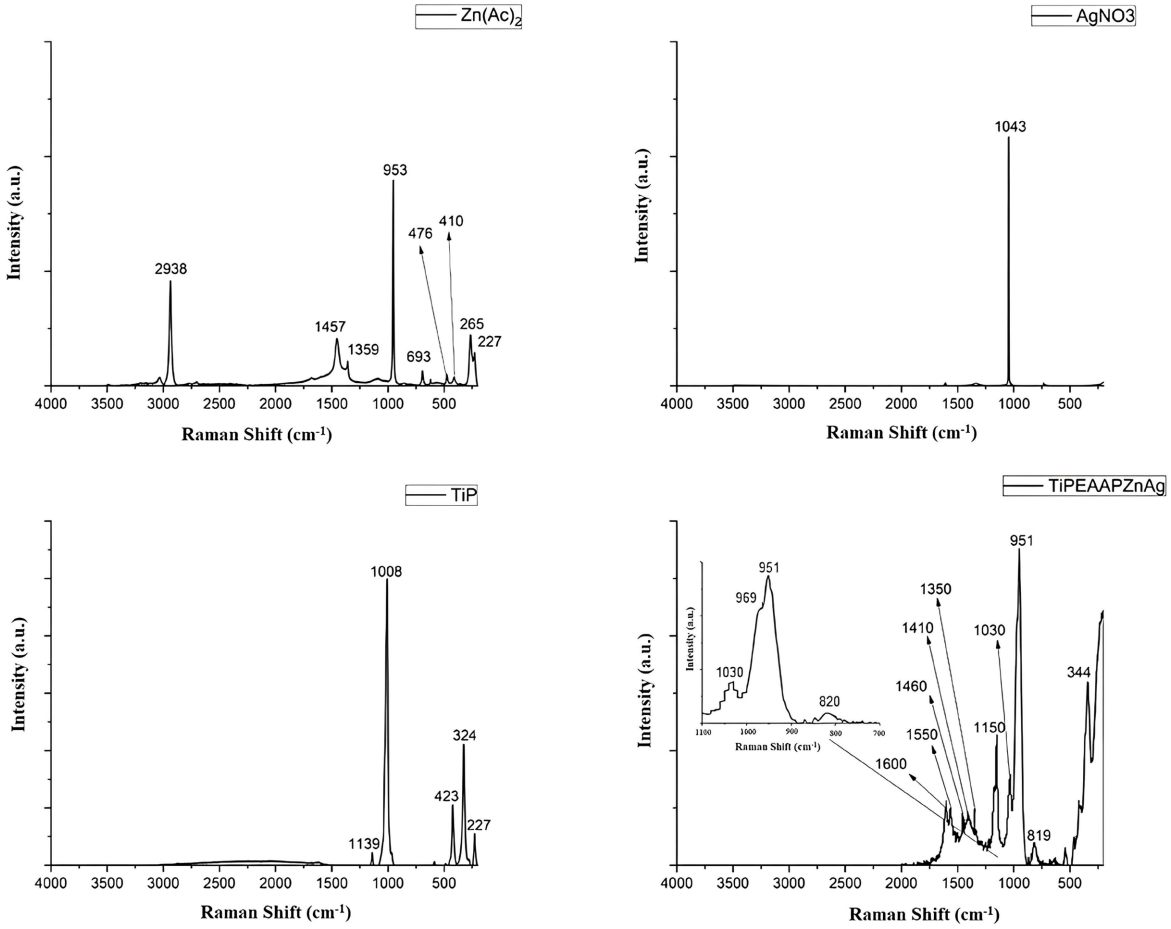

Figure 1. TiP, $Zn(Ac)_2$, $AgNO_3$ and TiPEAAPZnAg spectra.

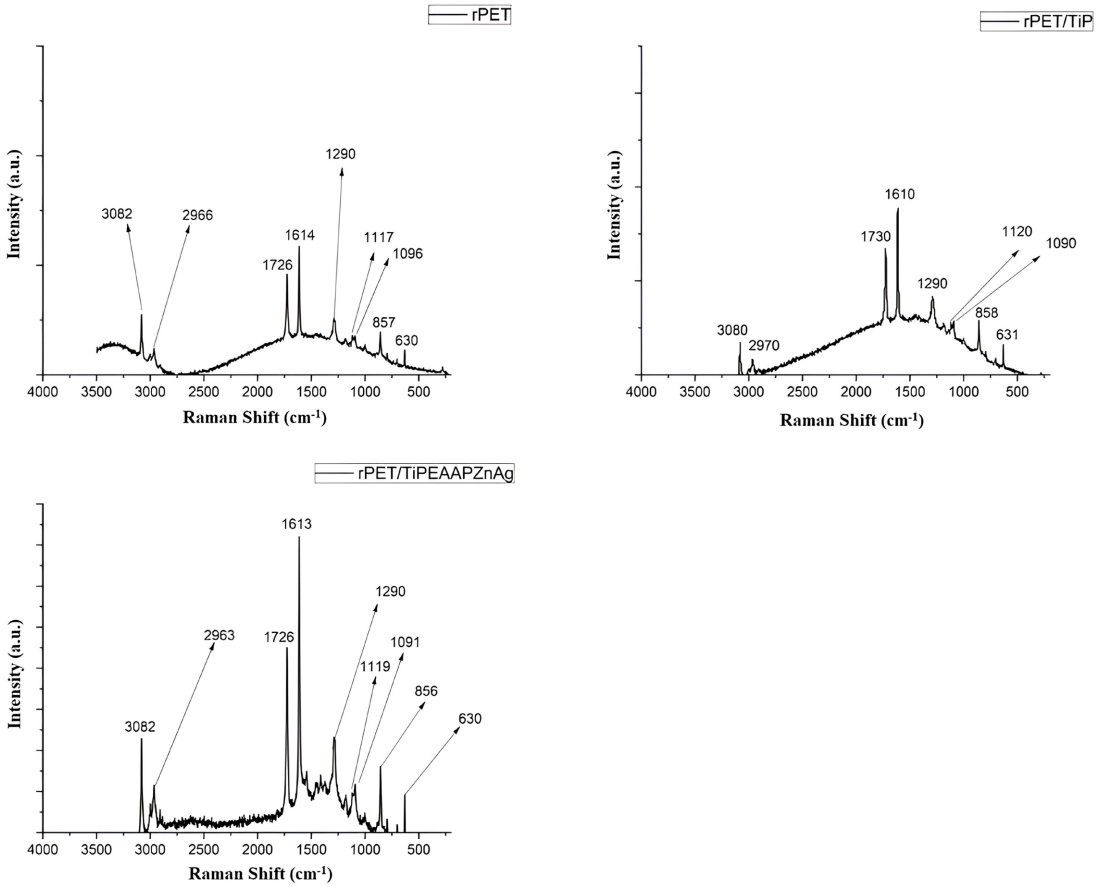

Figure 2. rPET, rPET/TiP and rPET/TiPEAAPZnAg spectra.

3.2. Hydrogen Nuclear Magnetic Resonance at Time Domain

Figure 3 presents the distribution domain curves of the samples. The rPET showed a rigid domain at 0.031 ms and a mobile domain at 0.167 ms. In rPET/TiP, both domains were observed to be displaced along the time axis. The lower domain increased the rigidity while the higher domain increased molecular mobility. The rPET/TiPEAAPZnAg revealed distribution domain curves very similar to those of rPET, but the slight narrowing at domain curves could indicate better affinity between polymer and filler. Mazur *et al*. studied the effect of commercial dimethyl dihydrogenated tallow ammonium cations-modifying montmorillonite (Cloisite® 20A, C20A) at a content of 5 - 10 wt.% in blends of poly (butylene succinate) (PBS)/poly (lactic acid) (PLA) [44]. Although with a high C20A content, the proton spin-lattice relaxation time (T_1) of the composite indicated a slight variation of the blend's molecular relaxation. Using time domain low field NMR, Jing *et al*. investigated the molecular mobility of poly (vinyl butyral) (PVB) plasticized with triethylene glycol bis (2-ethylhexanoate) (25 wt.% of TEG-EH) [45]. The evaluation of T_2 relaxation time showed a considerable increase in PVB molecular dynamics, ascribed to the plasticizing effect. The limited influence of the fillers on the molecular mobility of rPET composites could be attributed to ethylamine (a low-chain amine), which restricted the expansion of TiP interlayers, and to the

low filler content (only 1 wt.%) used in the composite preparation.

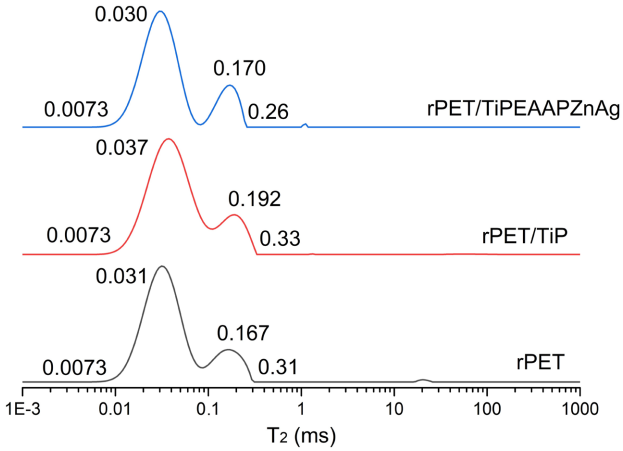

Figure 3. Samples' domain distribution curves.

3.3. Rheology

Figure 4 represents the evolution of storage modulus (G'), loss modulus (G") and complex viscosity (η^*), respectively. G' showed different behaviors above and below 2×10^1 rad/s. Below this threshold, the curves of rPET and rPET/TiPEAAPZnAg are practically superimposed. The curve of rPET/TiP showed a lower G' value. Above that limit, the curves showed a trend, indicating the rearrangement of fillers in the rPET/TiP composite promoted by the oscillatory work during the test. For G", all curves are superimposed indicating no apparent influence of composite processing and filler addition on the degradation of rPET chains. For all curves, complex viscosity (η^*) exhibited pseudoplastic behavior. Below $2 \times 10^{\circ}$ rad/s, the rPET and rPET/TiPEAAPZnAg curves were nearly superimposed. The rPET/TiP curve displayed a lower value of η^* due to the arrangement of filler in the composite. Above $2 \times 10^{\circ}$ rad/s, the curves tended to overlap. **Table 1** shows the behavior of G"/G' at different frequencies. The values of G"/G' converge at both frequencies with the profiles of G', G", and η^*. At 10° rad/s, for rPET and rPET/TiPEAAPZnAg, the G"/G' values were very close, while for rPET/TiP, G"/G' was too high due to the reduction of G'. At 10^2 rad/s, all G"/G' values were similar. Chowreddy *et al*. studied recycled PET/carbon nanotubes composites [46]. They observed an increase in G' and η^* with increasing filler concentration. It was deduced that the filler acted by hindering the flow of the PET and, therefore, increasing the complex viscosity. In another article, Chowreddy *et al*. prepared a nanocomposite of recycled PET/clay [47]. At a concentration of 1%, little variation of G', G" and η^* was registered. According to Litchfield and Baird, the aggregation of the filler's particles increases the distortion of the polymer flow lines, causing huge effects on the rheological properties [48]. Exfoliated or well-dispersed nanoparticles exhibit different rheological behavior compared to their agglomerated counterparts. Herein, the materials exhibited different rheologic behavior at low and high frequencies. At low frequencies, G' and viscosity curves

behaved according to the dispersion and distribution of each filler in the composites. At high frequencies, the rheologic behavior tended to be similar.

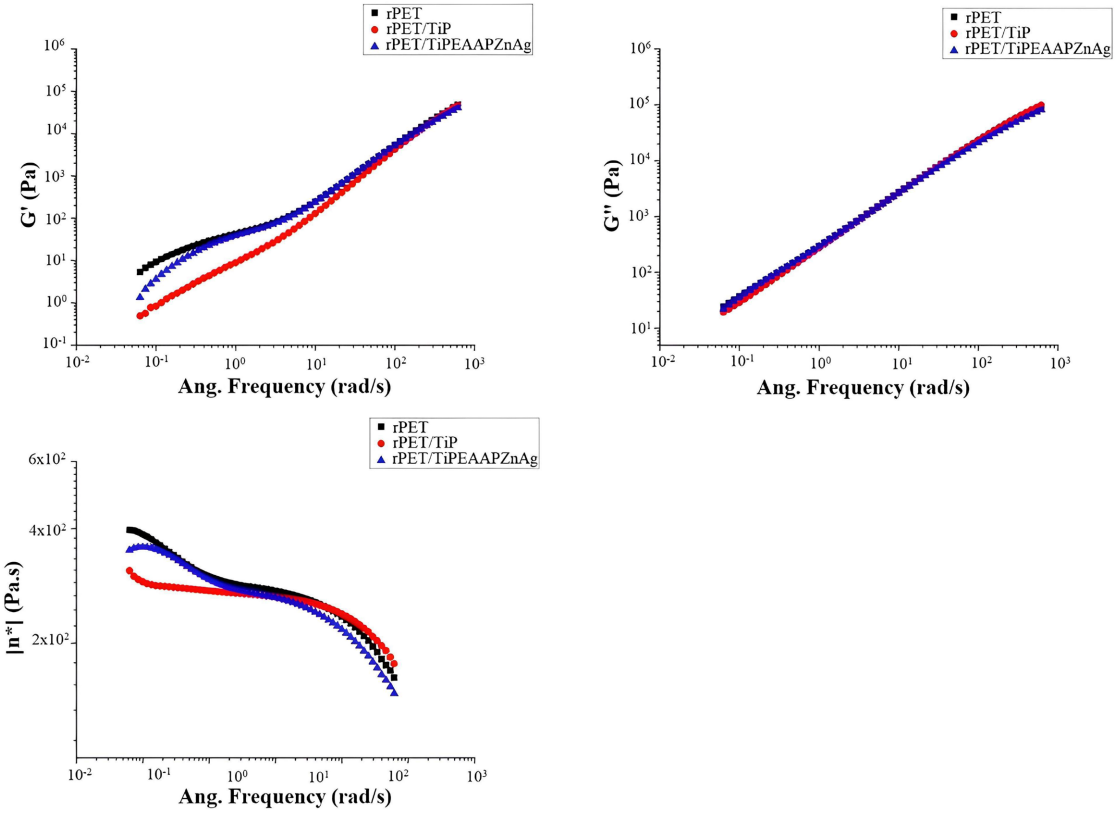

Figure 4. G', G" and η^* curves.

Table 1. Evaluation of G"/G' at different frequencies.

Sample	10° rad/s			10^2 rad/s		
	G'(Pa)	G" (Pa)	G"/G'	G'(Pa)	G" (Pa)	G"/G'
rPET	42.7	295.6	6.9	24,960	59,550	2.4
rPET/TiP	8.8	273.4	31.0	22,900	65,250	2.8
rPET/TiPEAAPZnAg	38.6	289.9	7.5	21,740	54,470	2.5

3.4. Ultraviolet Stabilization

Figure 5 displays the carbonyl index measurement. Although variations could be detected, they were within the experimental error, indicating stabilization in the applied conditions. Debska *et al.* investigated the effect of accelerated aging (UV radiation of 340 nm, 63˚C, simulating rain) on the physical and mechanical properties of composites based on plastic waste including recycled PET from beverage bottles [49]. They reported that until 500 hours of exposure, no color change or remarkable mechanical properties were achieved. Pires *et al.* investigated the action of nano zinc oxide (nZnO, 0 - 3 wt.%) as a shield for ultraviolet radiation of recycled PET/polycarbonate (rPET/PC, 80/20 wt./wt.%) blend [50]. The PET and

PC carbonyl indexes suggested that the UV damage was attenuated in the sample containing the highest content of nZnO. This result could suggest that the presence of TiP and TiPEAAPZnAg did not induce notable changes in rPET chains during processing.

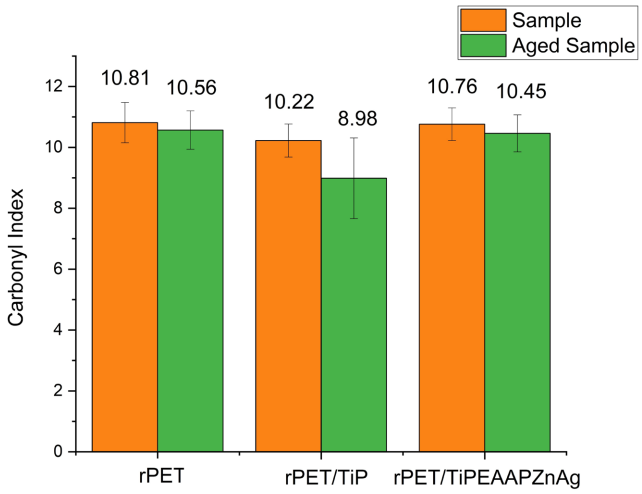

Figure 5. Samples' carbonyl index.

3.5. Polarized Optical Microscopy

Figure 6 shows POM images before and after crystallization, with and without polarized light. The sample film (sandwiched between sheets of glass) was heated to 260˚C, left for 1 minute to erase the thermal history, cooled up to 200˚C and held for 180 minutes. After that, the sample was cooled until 25˚C. For all samples, before and after the application of the crystallization protocol, the optical images seem to be similar. Viora *et al*. studied the crystallization of virgin and recycled PET [51]. POM images revealed variations in organizational spherulitic crystals between both PETs. For recycled PET, the final diameters of the spherulites were on the order of magnitude of 4 μm or even less. The result was associated with factors such as contaminants and shorter chain lengths, which limited the growth due to numerous active crystallization sites. In the study of the action of carbonate salts in the rPET crystallization kinetics, Xanthos *et al*. reported that PET has a low crystallization rate (10 μ/min) and nuclei formation when compared to polyethylene (5000 μ/min) [52]. Calcagno *et al*. investigated the effect of four types of montmorillonite—(2-5 wt.%, Cloisite: Na, 15 A (cationic modifier C18), 30 B (cationic modifier C16) and 10A (cationic modifier C14)—in nanocomposites based on PET [53]. They detected higher crystallization rates and smaller spherulites' size for nanocomposites than for pure PET. Through the POM analysis, no variation in nucleation and crystal size of rPET was observed. It was believed that ethylamine (a low chain amine) acted as a small intercalator for TiP interlayers, affecting the polymer/filler interaction to some extent. Also, the amount of filler (only 1 wt.%) could have contributed. This result corroborated the time domain NMR analysis.

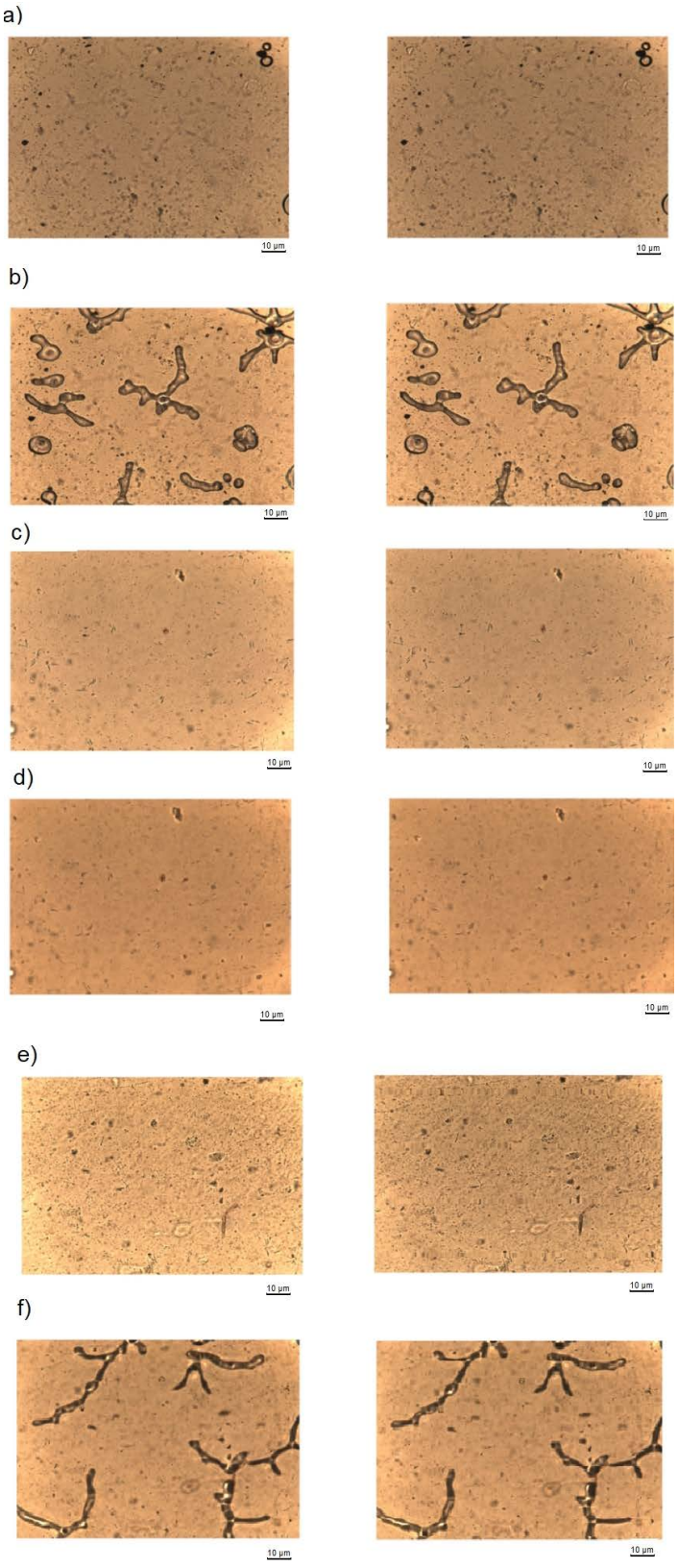

Figure 6. POM images: rPET before (a) and after crystallization (b); rPET/TiP before (c) and after crystallization (d); rPET/TiPEAAPZnAg before (e) and after (f) crystallization. Left column (without polarized light) and right column (with polarized light).

3.6. Dynamic-Mechanical Analysis

Figure 7 shows the curves of moduli (storage, E', and loss, E") and tangent delta (Tan δ). In the vitreous state, the E' value followed the sequence: rPET > rPET/TiPEAAPZnAg > rPET/TiP. After entering the rubbery state, the curves tended to overlap. The E" curves behaved similarly to those of E'. The maximum of the loss peak represents the glass transition temperature (T_g), which followed the rating: 83˚C, 86˚C and 88˚C for rPET > rPET/TiP > rPET/TiPEAAPZnAg, respectively. At the maximum of the Tan δ peak, no variation was observed, indicating that the damping characteristics of rPET were maintained. Yang *et al.* investigated the melting crystallization and thermal properties of composites based on recycled PET and graphene platelets [54]. The T_g increased and attained an invariable value in the range of 2 - 6 wt.% of graphene. In summary, the fillers caused some stiffening of the rPET amorphous phase, which could be attributed to some polymer/filler interaction. Also, the presence of fillers did not affect the damping characteristics of rPET.

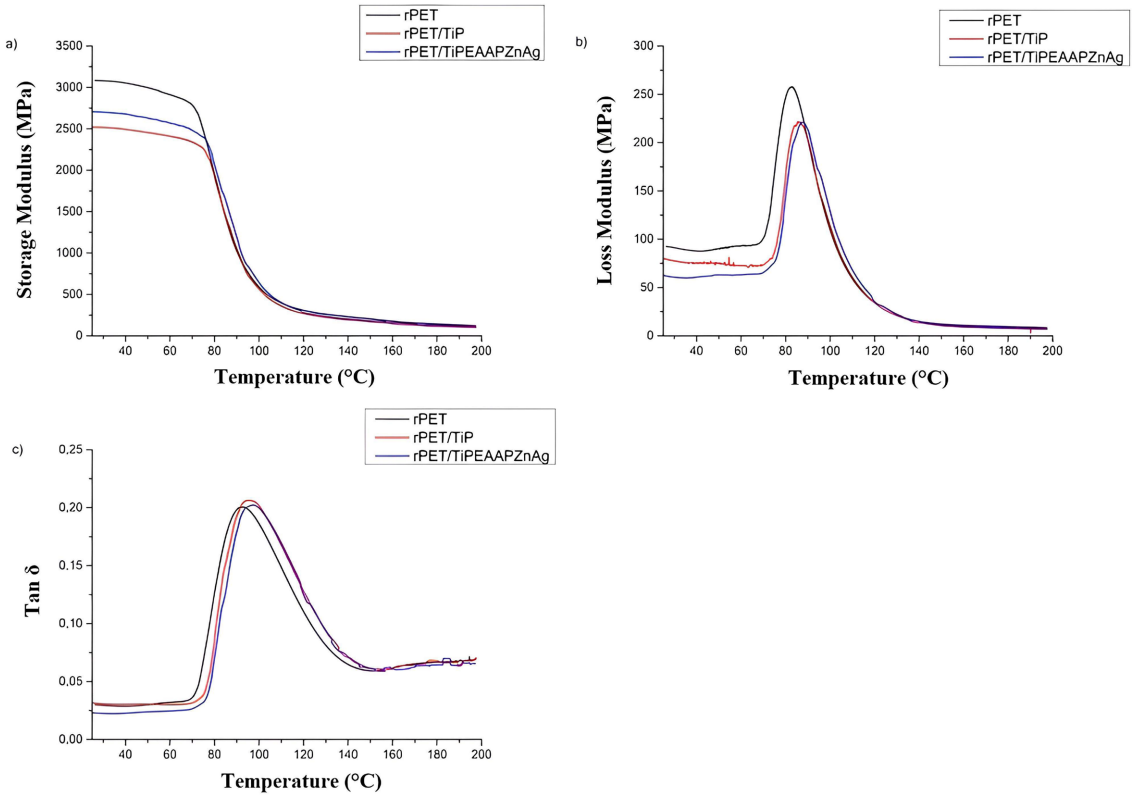

Figure 7. Storage modulus (a), loss modulus (b) and Tan δ (c).

3.7. Contact Angle

Figure 8 displays the contact angle assessment. Both fillers caused the lowering of the contact angle. Kusumocahyo *et al.* studied ultrafiltration membranes based on recycled PET filled with polyethylene glycol [55]. As the PEG concentration increased, the lowering of the contact angle was noticed due to the improvement of

hydrophilicity. For rPET/TiP, the decrease in contact angle could be attributed to the presence of P-O-H groups in the TiP surface, which probably increased the hydrophilicity. For rPET/TiPEAAPZnAg, the hydroxyl groups attached to TiP and the insertion of pyromellitic acid in the filler further improved the hydrophilicity.

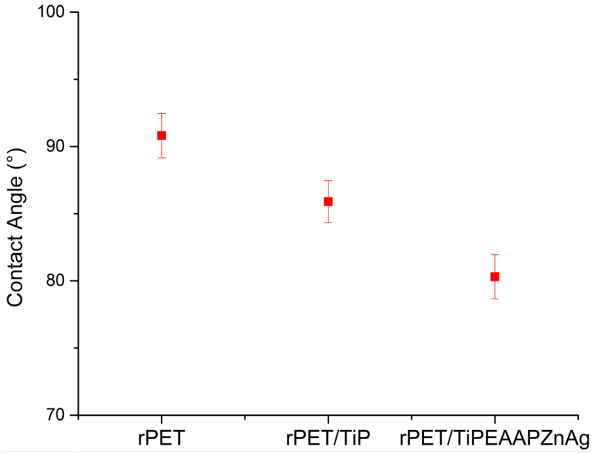

Figure 8. Contact angle of rPET and composites.

3.8. Lightfastness Measurement

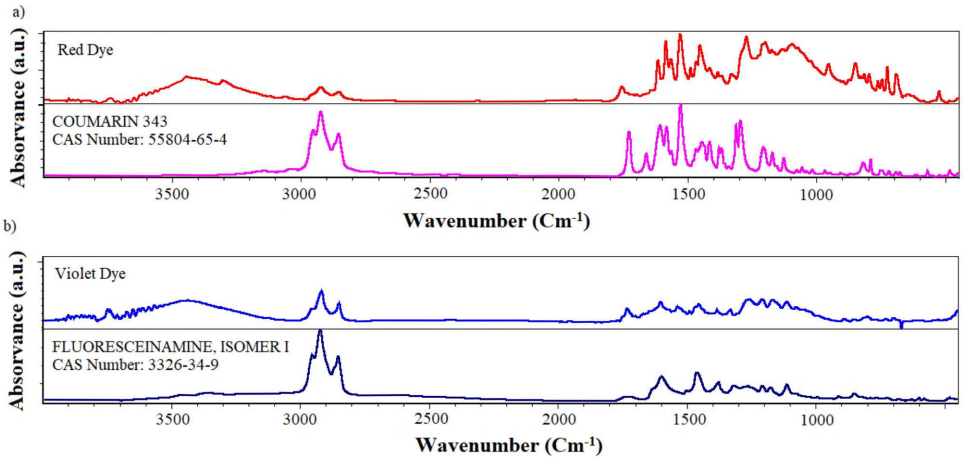

Figure 9. Infrared spectra of red(a) and violet dyes(b).

Firstly, some considerations about the chemical nature of dyes are provided. Figure 9 shows the infrared spectra of red and violet dyes. According to the equipment's spectrum collection, the red one presents similarity to the coumarin family and the blue one to fluorescein. The lightfastness test is appropriate for evaluating textile color retention (degree of fading). The grey scale of the lightfastness is rated between 1 - 5. Low grade (1) means that higher degree of fading while on the contrary, a higher value of lightfastness (5) represents excellent color retention [56]. Figure 10 shows the samples after incorporation of red and violet dyes. Table 2 shows the lightfastness measurement of rPET and composites. For all samples,

there was no variation in the degree of fading for both types of dyes. Gashti *et al*. reported that polymer substrate, physical state and concentration of dye and the presence of UV absorbers are factors which could affect the lightfastness of dyes [57]. Summarizing, it was possible to infer that the color retention could be attributed to some intermolecular interaction among polymer, filler, and dye.

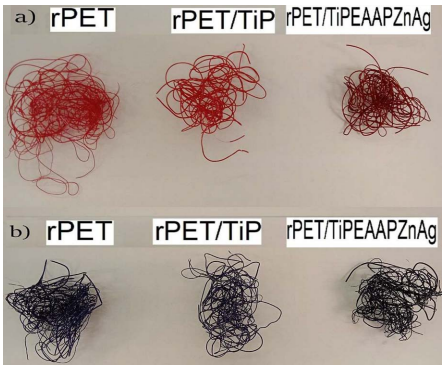

Figure 10. Filaments with different dyes: a) red dye; b) violet dye.

Table 2. Lightfastness of rPET and composites.

Composites	Color	
	Red	Blue
rPET	5	4-5
rPET/TiP	5	4-5
rPET/TiPEAAPZnAg	4	4-5

4. Conclusion

With attention focused on environmental sustainability, this work aimed to investigate the effects of nano-titanium phosphate, with or without chemical modification, on the properties of rPET. Some stiffening of the rPET amorphous phase was caused by the nano-fillers, which could be attributed to their nature. The decrease in the contact angle was attributed to the increased hydrophilicity, which is feasible for textile applications. Rheology, UV stabilization, POM and lightfastness were practically unaffected by the addition of fillers. The synthesis and consecutive modifications of the filler serve to improve the dispersion and distribution of the salts in the polymer matrix as well as to improve the interaction between polymer and filler. The work aligns with the goals established by the UN 2030 Agenda and supports the practicability of recycling plastic waste as an eco-friendly method. Work continues at the IMA laboratory seeking partnerships for microbiological evaluation and variations in experimental procedures related to intercalation and type of intercalant.

Acknowledgements

The authors thanks the Conselho Nacional de Desenvolvimento Científico e

Tecnológico (CNPq) and Coordenação de Aperfeiçoamento de Pessoal de Nível Superior (CAPES) Finance Code 1 and FAPERJ—Fundação Carlos Chagas Filho de Amparo à Pesquisa do Estado do Rio de Janeiro and Universidade Federal do Rio de Janeiro for the support to this research.

Data Availability Statement

All data generated or analyzed during this study are included in this published article.

Conflicts of Interest

On behalf of all authors, the corresponding author states that there is no conflict of interest.

References

[1] United Nations (2024) The Sustainable Development Agenda. https://www.un.org/sustainabledevelopment/development-agenda/

[2] European Commission (2024) Circular Economy Action Plan. https://environment.ec.europa.eu/strategy/circular-economy-action-plan_en

[3] Ciobanu, R.C., Aradoaei, M., Caramitu, A.R., Ion, I., Schreiner, C.M., Tsakiris, V., *et al*. (2023) Special Packaging Materials from Recycled Pet and Metallic Nano-Powders. *Polymers*, **15**, Article 3161. https://doi.org/10.3390/polym15153161

[4] Chaka, K.T., Ahmed, F.E., Zegeye, L.H. and Worku, B.G. (2022) Compressive Strength of Floor Tile Composites from Recycled Pet Reinforced with Natural Fibers. *Journal of Natural Fibers*, **20**, Article 2146249. https://doi.org/10.1080/15440478.2022.2146249

[5] Laria, J.G., Gaggino, R., Kreiker, J., Peisino, L.E., Positieri, M. and Cappelletti, A. (2020) Mechanical and Processing Properties of Recycled PET and LDPE-HDPE Composite Materials for Building Components. *Journal of Thermoplastic Composite Materials*, **36**, 418-431. https://doi.org/10.1177/0892705720939141

[6] Almahri, G., Madi, K., Alkaabi, F., Badran, Y., Shehadeh, K., ElHassan, A., *et al*. (2023) Characterization of Hybrid FRP Composite Produced from Recycled PET and CFRP. *Polymers*, **15**, Article 2946. https://doi.org/10.3390/polym15132946

[7] Kuété, M.A., Van Velthem, P., Ballout, W., Klavzer, N., Nysten, B., Ndikontar, M.K., *et al*. (2023) Eco-Friendly Blends of Recycled PET Copolymers with PLLA and Their Composites with Chopped Flax Fibers. *Polymers*, **15**, Article 3004. https://doi.org/10.3390/polym15143004

[8] Singh, A.K., Bedi, R. and Kaith, B.S. (2021) Composite Materials Based on Recycled Polyethylene Terephthalate and Their Properties—A Comprehensive Review. *Composites Part B*: *Engineering*, **219**, Article 108928. https://doi.org/10.1016/j.compositesb.2021.108928

[9] Lee, M., Kim, K., Chung, C.-W., Kim, W., Jeong, Y. and Lee, J. (2023) Mechanical Characterization of Recycled-PET Fiber Reinforced Mortar Composites Treated with Nano-SiO_2 and Mixed with Seawater. *Construction and Building Materials*, **392**, Article 131882. https://doi.org/10.1016/j.conbuildmat.2023.131882

[10] Duan, Z., Deng, Q., Liang, C., Ma, Z. and Wu, H. (2023) Upcycling of Recycled Plastic Fiber for Sustainable Cementitious Composites: A Critical Review and New Perspective. *Cement and Concrete Composites*, **142**, Article 105192.

https://doi.org/10.1016/j.cemconcomp.2023.105192

[11] Rhee, I., Lee, J.-S., Kim, Y.-A. and Kim, J.-M. (2023) Mechanical Properties of Cement Mortar with Gamma-Irradiated Recycled Plastic Powder, Pellet, and Fiber. *Results in Engineering*, **20**, Article 101614. https://doi.org/10.1016/j.rineng.2023.101614

[12] Weng, L. and Zhang, X. (2023) Recycling Polyester Fiber with Bio-Based Alginate Fiber into Fire-Safety Composite. *Polymer Degradation and Stability*, **217**, Article 110519. https://doi.org/10.1016/j.polymdegradstab.2023.110519

[13] Paredes, J., Castillo, W., Salinas, G., Erazo, H. and Guerrero, V.H. (2023) Optimization of Compression and Flexural Properties of Masonry Veneers with Recycled PET-1. *Polymers*, **15**, Article 1122. https://doi.org/10.3390/polym15051122

[14] Maladeniya, C.P., Tennyson, A.G. and Smith, R.C. (2023) Single-Stage Chemical Recycling of Plastic Waste to Yield Durable Composites via a Tandem Transesterification-Thiocracking Process. *Journal of Polymer Science*, **61**, 787-793. https://doi.org/10.1002/pol.20220686

[15] Zhang, S., Xu, W., Du, R., An, W., Liu, X., Xu, S., *et al*. (2023) Selective Depolymerization of PET to Monomers from Its Waste Blends and Composites at Ambient Temperature. *Chemical Engineering Journal*, **470**, Article 144032. https://doi.org/10.1016/j.cej.2023.144032

[16] Singh, A.K. and Bedi, R. (2023) Effect of Graphene Nanoplatelets on Fatigue Performance of Glass Fiber Reinforced Composite Materials Based on Recycled Polyethylene Terephthalate. *Composites Communications*, **40**, Article 101595. https://doi.org/10.1016/j.coco.2023.101595

[17] Kalaoglu-Altan, O.I., Karagüzel Kayaoğlu, B. and Trabzon, L. (2023) Fabrication and Characterization of Graphene-Loaded Recycled Poly (Ethylene Terephthalate) Electrospun Composite Nanofibrous Mats with Improved Thermal Conductivity. *Polymer Composites*, **45**, 709-721. https://doi.org/10.1002/pc.27809

[18] Nasir, N.H.M., Usman, F., Woen, E.L., Ansari, M.N.M., Supian, A.B.M. and Saloma, S. (2023) Microstructural and Thermal Behaviour of Composite Material from Recycled Polyethylene Terephthalate and Fly Ash. *Recycling*, **8**, Article 11. https://doi.org/10.3390/recycling8010011

[19] Lopez, C.V. and Smith, R.C. (2023) Chemical Recycling of Poly (Ethylene Terephthalate) via Sequential Glycolysis, Oleoyl Chloride Esterification and Vulcanization to Yield Durable Composites. *Materials Advances*, **4**, 2785-2793. https://doi.org/10.1039/D2MA00986B

[20] Moulai Arbi, Y., Mahmoudi, N. and Djebli, A. (2023) Manufacturing and Testing of Waste PET Reinforced with Sand Bricks. *Journal of Composite Materials*, **57**, 2513-2526. https://doi.org/10.1177/00219983231175203

[21] Adiyanto, O., Mohamad, E., Irianto, Jaafar, R., Faishal, M. and Rasyid, M.I. (2023) Optimization of PET Particle-Reinforced Epoxy Resin Composite for Eco-Brick Application Using the Response Surface Methodology. *Sustainability*, **15**, Article 4271. https://doi.org/10.3390/su15054271

[22] Maslova, M., Mudruk, N., Ivanenko, V. and Gerasimova, L. (2022) Highly Efficient Synthesis of Titanium Phosphate Precursor for Electroactive Materials. *Ceramics International*, **48**, 2257-2272. https://doi.org/10.1016/j.ceramint.2021.10.004

[23] Wang, C., Cheng, Q. and Wang, Y. (2018) Anion-Controlled Cation-Exchange Process: Intercalating α-Titanium Phosphate through Direct Ion Exchange with Alkylammonium Salts. *Inorganic Chemistry*, **57**, 3753-3760. https://doi.org/10.1021/acs.inorgchem.7b03030

[24] Amghouz, Z., García, J.R. and Adawy, A. (2022) A Review on the Synthesis and Current and Prospective Applications of Zirconium and Titanium Phosphates. *Eng*, **3**, 161-174. https://doi.org/10.3390/eng3010013

[25] Li, G., Wan, X., Xia, Y., Tuo, D., Qi, X., Wang, T., *et al*. (2023) Lamellar *α*-Zirconium Phosphate Nanoparticles Supported on N-Doped Graphene Nanosheets as Electrocatalysts for the Detection of Levofloxacin. *ACS Applied Nano Materials*, **6**, 17040-17052. https://doi.org/10.1021/acsanm.3c03162

[26] Mendes, L.C., Silva, D.F., Araujo, L.J. and Lino, A.S. (2014) Zirconium Phosphate Organically Intercalated/Exfoliated with Long Chain Amine. *Journal of Thermal Analysis and Calorimetry*, **118**, 1461-1469. https://doi.org/10.1007/s10973-014-4056-0

[27] Albitres, G.A.V., Cestari, S.P., Malafaia Macedo, K.R., Cruz, M.O., Filho, M.F., *et al*. (2019) Poly(Ethylene Terephthalate)/Titanium Phosphate Nanocomposites: Effect of Fillers on Thermal, Crystallographic Diffraction, Molecular Mobility, and UV-Vis Absorption. *Journal of Thermoplastic Composite Materials*, **35**, 891-909. https://doi.org/10.1177/0892705719886926

[28] Garcia, E.E., Freitas, D.F., Cestari, S.P., Coval, D.R., Mendes, L.C. and Albitres, G.A. (2019) Zirconium Phosphate Changing Hygroscopicity of Polyamide-6 in Nanocomposites PA-6/ZRP. *Journal of Thermal Analysis and Calorimetry*, **139**, 293-303. https://doi.org/10.1007/s10973-019-08396-1

[29] Albitres, G.A.V., Garcia, E.E., Soares, C., Freitas, D., Neto, R.C. and Mendes, L.C. (2024) Post-Consumer High Density Polyethylene/Zirconium Phosphate and Aluminum Hydroxide Composites: Assessment of Physico-Mechanical and Flame Retardancy Properties. *Journal of Composite Materials*, **58**, 489-503. https://doi.org/10.1177/00219983231226278

[30] Garcia, E.E., Albitres, G.A.V., Freitas, D.F., Mariano, D.M. and Mendes, L.C. (2022) Zinc and Silver Salts-Containing Lamellar Titanium Phosphate: A Multifunctional Filler. *Materials Sciences and Applications*, **13**, 366-388. https://doi.org/10.4236/msa.2022.136021

[31] Mariano, D.M., Freitas, D.F., Albitres, G.A.V., Mendes, L.C. and Tavares, M.I. (2023) Incorporation of Nano-Zinc Oxide in Lamellar Zirconium Phosphate: Synthesis and Characterization. *Materials Sciences and Applications*, **14**, 346-361. https://doi.org/10.4236/msa.2023.146022

[32] Freitas, D.F., Albitres, G.A.V., Mariano, D.M., Cestari, S.P. and Mendes, L.C. (2022) Mechanical, Thermal, Rheological Assessment of Polyamide-6 Reinforced Composites by Addition of Lamellar Zirconium Phosphate. *Journal of Thermoplastic Composite Materials*, **36**, 2600-2622. https://doi.org/10.1177/08927057221102858

[33] Gültekin, D. and Akbulut, H. (2016) Raman Studies of ZnO Products Synthesized by Solution-Based Methods. *Acta Physica Polonica A*, **129**, 803-805. https://doi.org/10.12693/APhysPolA.129.803

[34] Conterosito, E., Croce, G., Palin, L., Boccaleri, E., van Beek, W. and Milanesio, M. (2012) Crystal Structure and Solid-State Transformations of Zn-Triethanolamine-Acetate Complexes to ZnO. *CrystEngComm*, **14**, 4472-4477. https://doi.org/10.1039/c2ce06468e

[35] Yahia, S.B., Znaidi, L., Kanaev, A. and Petitet, J.P. (2008) Raman Study of Oriented ZnO Thin Films Deposited by Sol-Gel Method. *Spectrochimica Acta Part A*: *Molecular and Biomolecular Spectroscopy*, **71**, 1234-1238. https://doi.org/10.1016/j.saa.2008.03.032

[36] Hou, Y., Pan, Y., Dong, C. and Nie, B. (2020) Direct Transformation of $AgNO_3$ Com-

plex Encapsulated Fullerene (C_{60}) Microcrystal on Solid Silver Nitrate Crystal without Organic Ligands. *Applied Organometallic Chemistry*, **34**, e5978. https://doi.org/10.1002/aoc.5978

[37] Slade, R. (1997) The Isomorphous Acid Salts α-$ZR(HPO_4)_2{\cdot}H_2O$, α-$Ti(HPO_4)_2{\cdot}H_2O$ and α-Zr $(HAsO_4)_2{\cdot}H_2O$ Comparative Thermochemistry and Vibrational Spectroscopy. *Solid State Ionics*, **96**, 9-19. https://doi.org/10.1016/S0167-2738(97)00012-X

[38] Janusz, W., Khalameida, S., Skwarek, E., Skubiszewska-Zięba, J., Sydorchuk, V. and Charmas, B. (2018) Modification of Titanium Phosphate Precipitated from Titanylsulfate. *Journal of Thermal Analysis and Calorimetry*, **135**, 2925-2934. https://doi.org/10.1007/s10973-018-7611-2

[39] Diniz, R., De Abreu, H.A., De Almeida, W.B., Fernandes, N.G. and Sansiviero, M.T.C. (2005) Vibrational Spectra of Na, K, Mn^{2+}, Ni^{2+} and Zn^{2+} Salts of 1,2,4,5-Benzenetetracarboxylic (Pyromellitic) Acid—A Short Hydrogen Bond Evidence. *Spectrochimica Acta Part A*: *Molecular and Biomolecular Spectroscopy*, **61**, 1747-1757. https://doi.org/10.1016/j.saa.2004.07.005

[40] Pan, Q., Zheng, Y., Tong, Z., Shi, L. and Tang, Y. (2021) Novel Lamellar Tetrapotassium Pyromellitic Organic for Robust High-Capacity Potassium Storage. *Angewandte Chemie International Edition*, **60**, 11835-11840. https://doi.org/10.1002/anie.202103052

[41] Peñalver, R., Zapata, F., Arroyo-Manzanares, N., López-García, I. and Viñas, P. (2022) Raman Spectroscopic Strategy for the Discrimination of Recycled Polyethylene Terephthalate in Water Bottles. *Journal of Raman Spectroscopy*, **54**, 107-112. https://doi.org/10.1002/jrs.6457

[42] Jin, N., Song, Y., Ma, R., Li, J., Li, G. and Zhang, D. (2022) Characterization and Identification of Microplastics Using Raman Spectroscopy Coupled with Multivariate Analysis. *Analytica Chimica Acta*, **1197**, Article 339519. https://doi.org/10.1016/j.aca.2022.339519

[43] Zhu, C., Tong, N., Song, L. and Zhang, G. (2015) Investigation of Raman Spectra of Polyethylene Terephthalate. *International Symposium on Photonics and Optics*, **9656**, 72-76. https://doi.org/10.1117/12.2205157

[44] Mazur, L.P., Reis, F.R., Felix, S.B.R., Henrique, S.P., Barcelos, C.T., Gurgel, A.V.M., *et al*. (2024) Development of Novel Biopolymer Membranes by Electrospinning as Potential Adsorbents for Toxic Metal Ions Removal from Aqueous Solution. *Journal of Molecular Liquids*, **395**, Article 123782. https://doi.org/10.1016/j.molliq.2023.123782

[45] Jing, L.V., Chen, X., Wu, Z.-S., Li, Y.-H. and Chen, W. (2023) Chain Dynamics Heterogeneity in Plasticized Poly(Vinyl Butyral) (PVB) as Elucidated by Solid-State NMR. *Chinese Journal of Polymer Science*, **42**, 113-124. https://doi.org/10.1007/s10118-023-3017-0

[46] Chowreddy, R.R., Nord-Varhaug, K. and Rapp, F. (2018) Recycled Polyethylene Terephthalate/Carbon Nanotube Composites with Improved Processability and Performance. *Journal of Materials Science*, **53**, 7017-7029. https://doi.org/10.1007/s10853-018-2014-0

[47] Chowreddy, R.R., Nord-Varhaug, K. and Rapp, F. (2019) Recycled Poly(Ethylene Terephthalate)/Clay Nanocomposites: Rheology, Thermal and Mechanical Properties. *Journal of Polymers and the Environment*, **27**, 37-49. https://doi.org/10.1007/s10924-018-1320-6

[48] Litchfield, D.W. and Baird, D.G. (2006) The Rheology of High Aspect Ratio Nano-Particle Filled Liquids. *Rheology Reviews*, **1**, 1-60.

[49] Dębska, B., Caetano, M.A. and Brigolini Silva, G.J. (2024) Study of the Influence of Accelerated Aging on the Physical and Mechanical Properties of Polymer Composites Containing Rubber, Polyethylene and Poly(Ethylene Terephthalate) Waste. *Journal of Cleaner Production*, **444**, Article 141273. https://doi.org/10.1016/j.jclepro.2024.141273

[50] Pires, H.M., Mendes, L.C., Cestari, S.P., Cucinelli Neto, R.P., Rodrigues, D.C. and Mattos, G.C. (2016) NZNO as Barrier to Ultraviolet Radiation on rPET/PC Nanocomposites. *Journal of Nanoscience and Nanotechnology*, **16**, 9987-9996. https://doi.org/10.1166/jnn.2016.12080

[51] Viora, L., Combeau, M., Pucci, M.F., Perrin, D., Liotier, P.-J., Bouvard, J.-L., *et al.* (2023) A Comparative Study on Crystallisation for Virgin and Recycled Polyethylene Terephthalate (PET): Multiscale Effects on Physico-Mechanical Properties. *Polymers*, **15**, Article 4613. https://doi.org/10.3390/polym15234613

[52] Xanthos, M., Baltzis, B.C. and Hsu, P.P. (1997) Effects of Carbonate Salts on Crystallization Kinetics and Properties of Recycled Poly(Ethylene Terephthalate). *Journal of Applied Polymer Science*, **64**, 1423-1435. https://doi.org/10.1002/(SICI)1097-4628(19970516)64:7<1423::AID-APP22>3.0.CO;2-W

[53] Calcagno, C.I.W., Mariani, C.M., Teixeira, S.R. and Mauler, R.S. (2007) The Effect of Organic Modifier of the Clay on Morphology and Crystallization Properties of PET Nanocomposites. *Polymer*, **48**, 966-974. https://doi.org/10.1016/j.polymer.2006.12.044

[54] Yang, B., Chen, J., Su, L.-F., Miao, J.-B., Chen, P., Qian, J.-S., *et al.* (2019) Melt Crystallization and Thermal Properties of Graphene Platelets (GNPs) Modified Recycled Polyethylene Terephthalate (RPET) Composites: The Filler Network Analysis. *Polymer Testing*, **77**, Article 105869. https://doi.org/10.1016/j.polymertesting.2019.04.016

[55] Kusumocahyo, S.P., Ambani, S.K., Kusumadewi, S., Sutanto, H., Widiputri, D.I. and Kartawiria, I.S. (2020) Utilization of Used Polyethylene Terephthalate (PET) Bottles for the Development of Ultrafiltration Membrane. *Journal of Environmental Chemical Engineering*, **8**, Article 104381. https://doi.org/10.1016/j.jece.2020.104381

[56] MacEvoy, B. (2024) Paints. http://www.handprint.com/HP/WCL/pigmt6.html#lightfast

[57] Gashti, M.P., and Moradian, S. (2012) Effect of Nanoclay Type on Dyeability of Polyethylene Terephthalate/Clay Nanocomposites. *Journal of Applied Polymer Science*, **125**, 4109-4120. https://doi.org/10.1002/app.35493